Supporting Information

Uncovering the Lead Formate Crystallization in Oil-Based Paintings

Silvie Švarcová[a]*, Eva Kočí[a], Petr Bezdička[a], Silvia Garrappa[a], Libor Kobera[b], Jiří Plocek[a], Jiří Brus[b], Martin Šťastný[a] and David Hradil[a,c]

[a]Institute of Inorganic Chemistry of the Czech Academy of Sciences, Husinec-Řež 1001, 250 68 Husinec-Řež, Czech Republic

[b]Institute of Macromolecular Chemistry of the Czech Academy of Sciences, Heyrovského nám. 2, 162 06 Praha 6, Czech Republic

[c]Academy of Fine Arts in Prague, ALMA Laboratory, U Akademie 4, 170 22, Prague 7, Czech Republic

e-mails: svarcova@iic.cas.cz, koci@iic.cas.cz, bezdicka@iic.cas.cz, garrappa@iic.cas.cz, kobera@imc.cas.cz, plocek@iic.cas.cz, brus@imc.cas.cz, stastny@iic.cas.cz, hradil@iic.cas.cz

*corresponding author: e-mail: svarcova@iic.cas.cz, phone number: +420 311 236 937

Table of Contents

The characterization of the starting minium pigment

X-ray powder diffarction

The phase purity of the pigment minium (Pb_3O_4, Aldrich, prod. # 241547-100G, lot # BCBV9427) was confirmed by XRPD. Data were collected on an XPertPRO MPD diffractometer in Bragg-Brentano geometry with the Cu radiation (40 kV, 30 mA), Soller slits of 0.02 rad, divergence slit 0.5 deg, antiscatter slit 0.5 deg, Ni filter and a PIXCel linear position sensitive detector. Measured in the angular range of 10 to 130 deg 2theta with the step of 0.0131 deg. and 1000s per step (producing a scan of about 10 hours 11 minutes). The XRPD pattern is shown in Fig. S1.

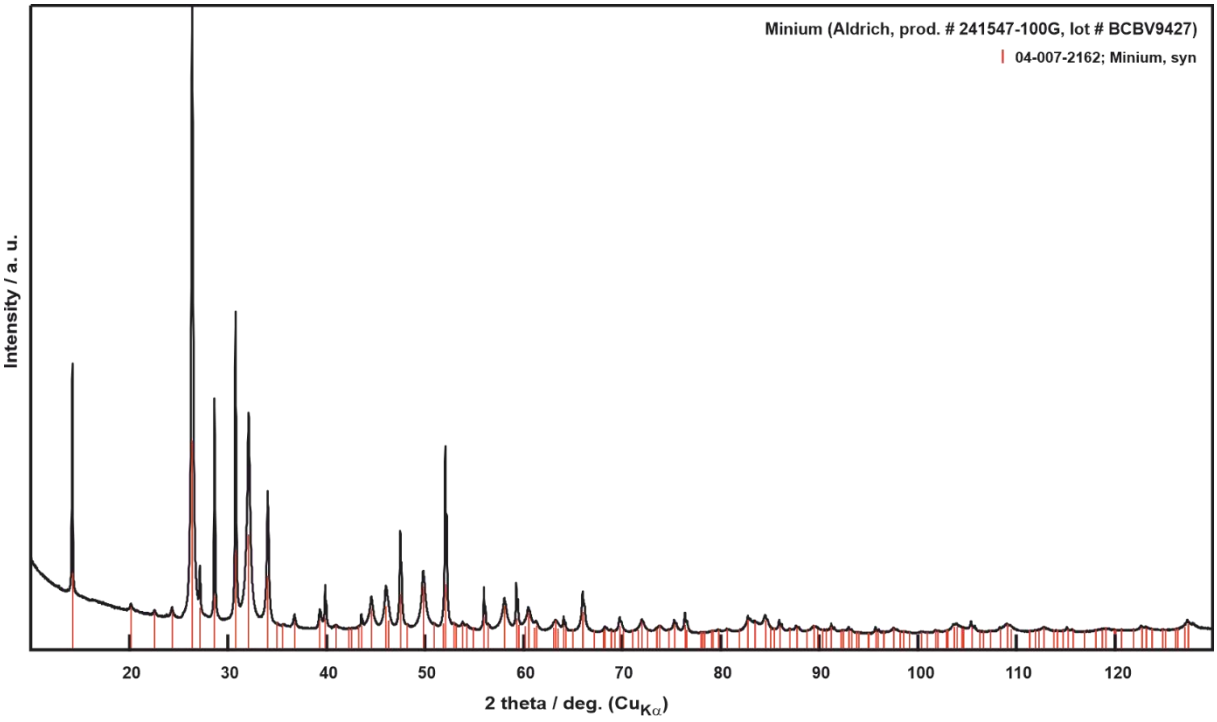

Fig. S1 XRPD pattern of the starting minium pigment.

The Rietveld refinement

A Profex / BGMN software was used for the Rietveld refinement with the structural model of minium based on the structural model of Gavarri and Weigel [1], (ICSD # 4106). This refinement confirmed that the sample of minium produced by Aldrich was found to be a phase pure compound. On contrary, we had to use a bimodal distribution of crystallite sizes as the sample was composed of larger crystals and nanocrystals. A complex anisotropic micro-strain was refined (see Leinenweber and Dinnebier [2]). We have observed the mean crystallite sizes of about 626 nanometers and 80 nanometers respectively. This result was also confirmed by the electron microscopy (SEM) and measurements of distribution of particle sizes by laser light scattering.

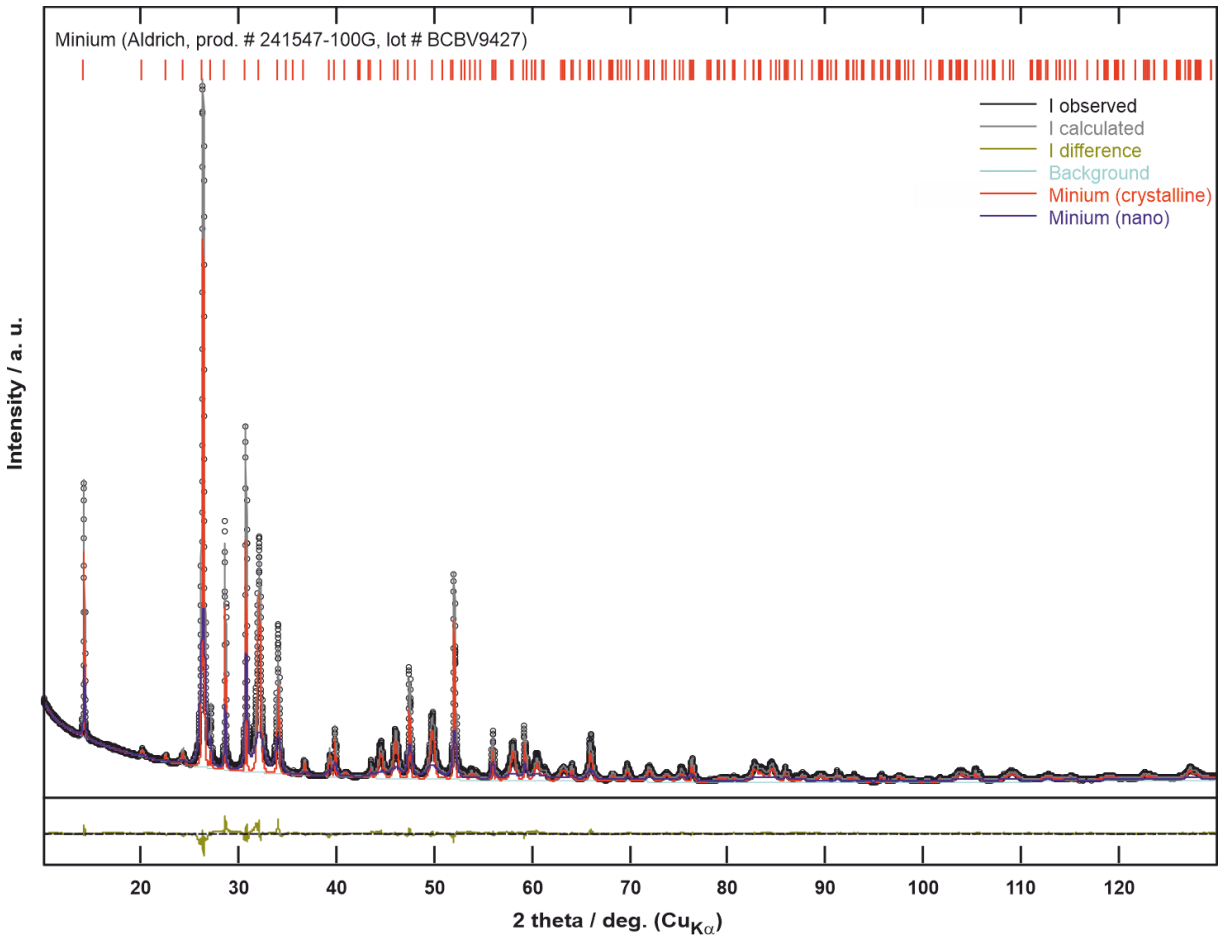

Fig. S2 The Rietveld refinement of the XRPD pattern of the starting minium pigment.

Particle size analysis

Particle size distribution of minium was measured by laser diffraction analyzer Bettersizer S3. The powder sample was initially dispersed in 1% solution of sodium pyrophosphate; this suspension was sonicated for 3 min and then added to water used as measuring medium. The results were evaluated by help of Mie method. The results are plotted in Fig. S3.

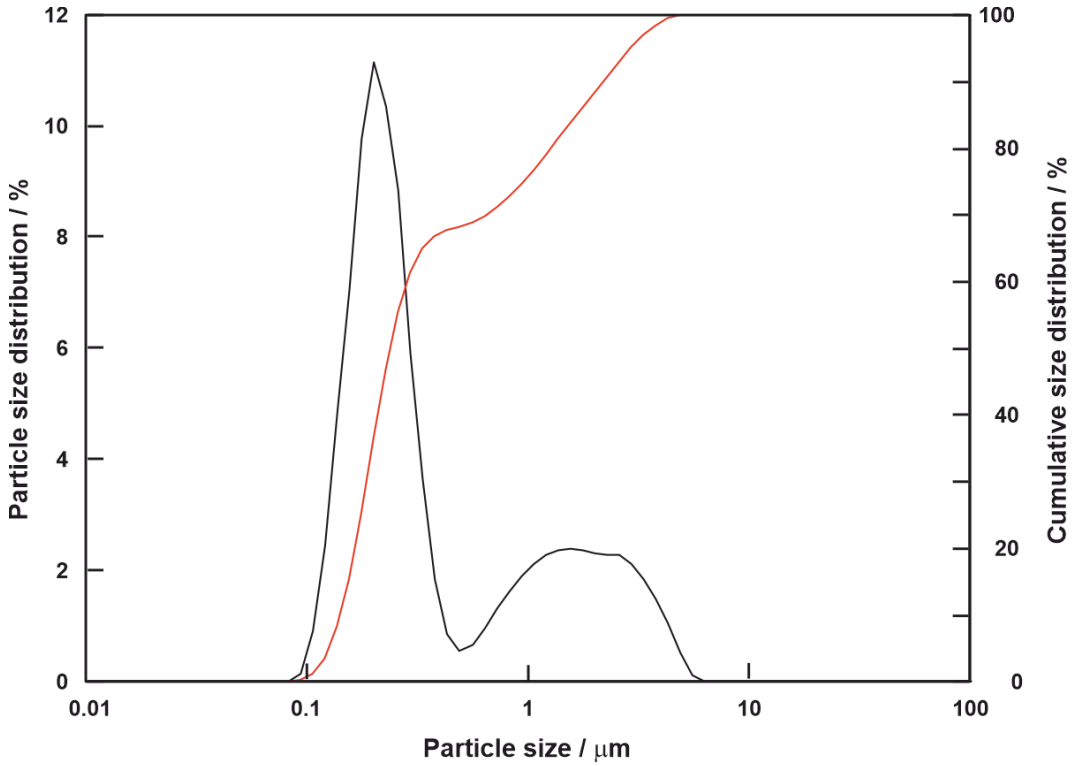

Fig. S3 The particle size distribution (black curve) and the cumulative size distribution (red curve) of minium.

Scanning electron microscopy

The SEM images were obtained on FEI Nova NanoSEM450 in a High-Vacuum mode with a Through Lens detector using accelerating voltage 5 kV. The sample was not coated for the measurement.

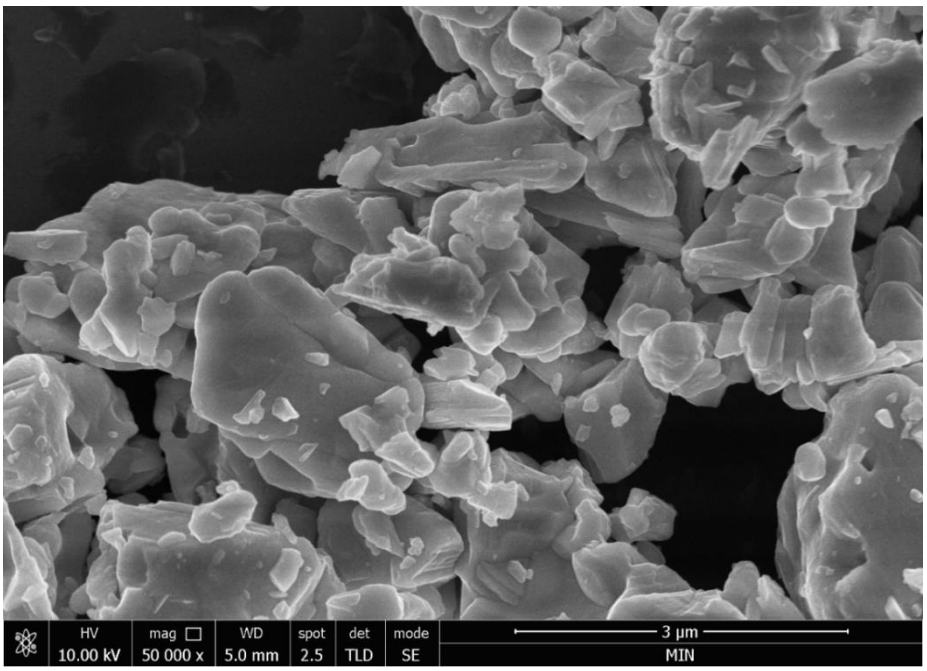

Fig. S4 SEM image of the grains of the minium pigment.

XRD-based calculation of current concentration of Pb-phases in model samples

For comparison of reaction rates of lead formate crystallization or minium reactions with various oil media, the comparison of relative diffraction intensities was chosen as an appropriate approximation for this type of *in situ* experiments to avoid admixing of other substances which could serve, on the one hand, as internal standards, however, on the other hand, they could affect negatively the relations in the paint films. The integral intensity of diffraction lines of a particular phase is proportional to its weight fraction the mixture, thus the current concentration of the phase can be estimated by plotting the relative intensity of a representative diffraction line to the reaction time.

Model paints

The integral intensities of the diffraction lines 110 at 16.9° 2θ $Cu_{K\alpha}$ for $Pb(HCOO)_2$ and 110 at 14.2° 2θ $Cu_{K\alpha}$, Pb_3O_4, respectively, were related to the integral intensity of Pb_3O_4 (110 at 14.2° 2θ $Cu_{K\alpha}$) in the XRD pattern for t = 0 because Pb_3O_4 is consumed by the formation of $Pb(HCOO)_2$ and Pb-soap phase for t > 0. Then the relative abundances of neo-formed $Pb(HCOO)_2$ as well as decrease of Pb_3O_4 can be compared each other.

The procedure for calculation of the relative abundances of neo-formed lead soaps has to be modified with respect to the non-crystalline character of the phase which is represented in XRD patterns by a broad hump at very low angles. A region from 1 to 10° 2θ $Cu_{K\alpha}$, in which the growing hump is detected within the time and where is no diffraction line of other crystalline phases in paint samples, was selected for calculation of integral intensities. The first XRD pattern collected at t = 0 was used as a background, which was subtracted from all subsequent diffraction patterns for t > 0. The difference corresponds to the relative increase of the concentration of lead soap phase in the particular mixture with time.

$$I_r(t) = \frac{I(t) - I(t=0)}{I(t=0)}$$

$I_r(t)$ – relative intensity of lead soap for time t
I(t) – intensity of lead soap for time t
I(t=0) – intensity of lead soap for time t=0
I(t) was calculated using HighScorePlus software package with the function “sum of observed intensity” for a region from 1 to 10° 2θ $Cu_{K\alpha}$.

Vapor experiments

The integral intensities of the diffraction lines 110 at 16.9° 2θ $Cu_{K\alpha}$ for $Pb(HCOO)_2$ and 110 at 14.2° 2θ $Cu_{K\alpha}$, Pb_3O_4, respectively, were related to the integral intensity of Pb_3O_4 (110 at 14.2° 2θ $Cu_{K\alpha}$) in the XRD pattern for t = 0 because Pb_3O_4 is consumed by the formation of $Pb(HCOO)_2$ for t > 0. Then the relative abundances of neo-formed $Pb(HCOO)_2$ as well as decrease of Pb_3O_4 can be compared each other.

Calculated NMR parameters

The ^{13}C and ^{207} Pb NMR parameters were performed using Amsterdam Density Functional (ADF 2017.111) program package.[3-5] The density functional BP86 –D3 at TZP basis set was used [6]. Relativistic effect ZORA/spin-orbit level.[7-9] The ^{13}C NMR and ^{207}Pb NMR chemical shielding calculations were performed on asymmetric unit and prepared cluster of $Pb(COOH)_2$ (CCCD deposit number 925259), respectively. Calculated NMR parameters are summarized in **Table S1**.

Table S1. DFT/ZORA calculated data of ^{207}Pb and ^{13}C chemical shifts of lead formate

Nuclei	σ^{calc} (ppm)[a]	δ_{iso} (ppm)[b]	Ω (ppm)	κ
^{207}Pb	8651.8	-716[a]	603	0.62
^{13}C	-16.79	164.3[b]	---	---
	-22.92	158.2[b]	---	---

[a] σ^{calc} (^{207}Pb) = 1.17 δ_{iso} + 7814; [b] δ_{iso} (^{13}C) = σ^{calc} + 181.1

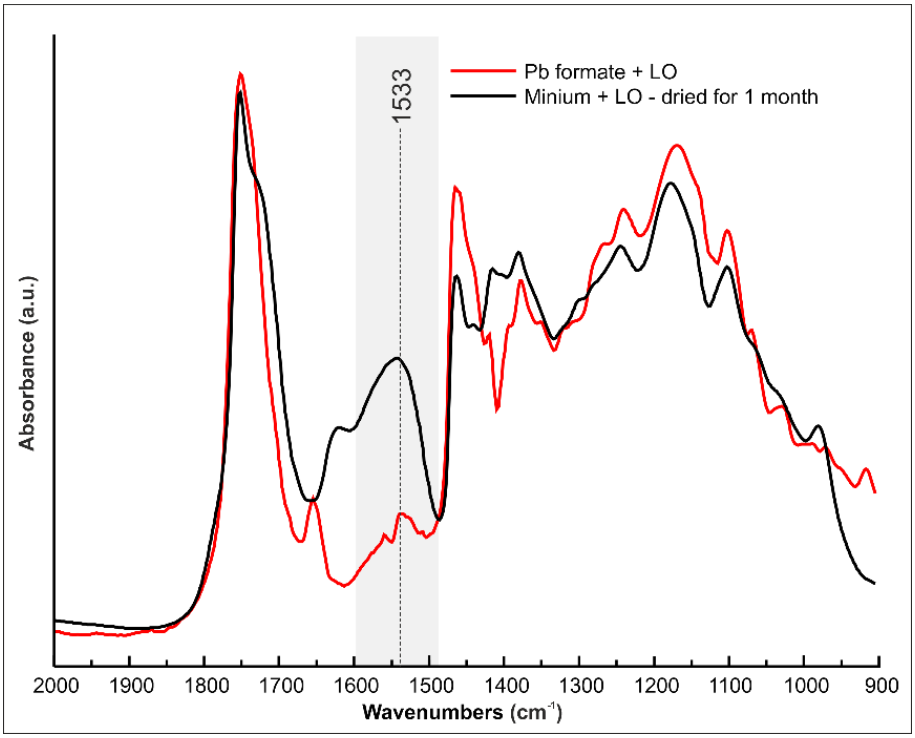

Fig. S5 Comparison of FTIR spectra of the fresh mixture consisted of synthetic lead formate and linseed oil (red line) with studied model paint after 1 moth of drying (black line). Apparently, the broad carboxylate band around 1530 cm^{-1} (corresponding to the Pb-ionomer) overlaps the weaker signal of crystalline lead formate.

Determination of fatty acids in drying oils

The fatty acid profiles of the drying oils used were analysed by gas chromatography with flame ionisation detector (GC-FID) according to a certified procedure in the Metrological and Testing Laboratory of University of Chemistry and Technology Prague (Testing laboratory 1316.2 accredited by the CAI according to the EN ISO/IEC 17025:2005). The determined fatty acids are given in **Table S2**.

Table S2. Composition of fatty acids in oils (weight %)

Fatty acid[a]	Linseed oil	Poppy-seed oil	Stand oil	Walnut oil
Palmitic (C16:0)	4.72	6.55	10.68	6.01
Stearic (C18:0)	3.17	3.68	8.58	2.64
Vaccenic (c18:1n11c)	0.97	1.25	0	1.29
Oleic (C18:1n9c)	13.65	19.19	26.34	13.3
Linoleic (C18:2n6c)	16.13	60.51	4.47	57.7
α-linolenic (C18:3n3)	54.75	0.18	0	11.6
γ-linolenic (C18:3n3)	0.18	0	3.54	0.56
Behenic (C22)	0.13	0.36	0	
Elaidic (C18:1n9t)			2.74	

[a]Fatty acids of concentration <1% are omitted

GC-MS analysis of oil vapors

Table S3. Chromatographic conditions for the detection of methanol, formaldehyde and formic acid in oil vapors

Hardware, Software	JEOL JMS-Q1000GC mass spectrometer with Agilent 6890N gas chromatograph. The collection of EI spectra and their evaluation was performed using the EI library NovaSpec ™ spectra
Mobile phase (carrier gas)	Helium (99,9999%)
Column	HP-5 19091J-413 (5%-Phenyl-methylpolysiloxan, 30 m × 0.32 mm I.D. × 0.25 µm)

Gas chromatograph (GC)		***Mass spectrometer (MS)***	
Injection unit temperature	250 °C	Interface temperature	250 °C
Column oven temperature	Initial: 50 °C (3 min hold time) → 240 °C (10 °C/min), 20 min (hold time)	Ion source temperature	200 °C
Injection mode	Split (50:1)	Measurement mode	Scan
Control mode	Linear velocity (2 ml/min)	Measurement range	m/z 10 to 100
Carrier gas	Helium	Resolution	1
Injection volume	1 µL	Ionization method	EI
		Ionization energy	70 eV
		Ionization current	150 µA

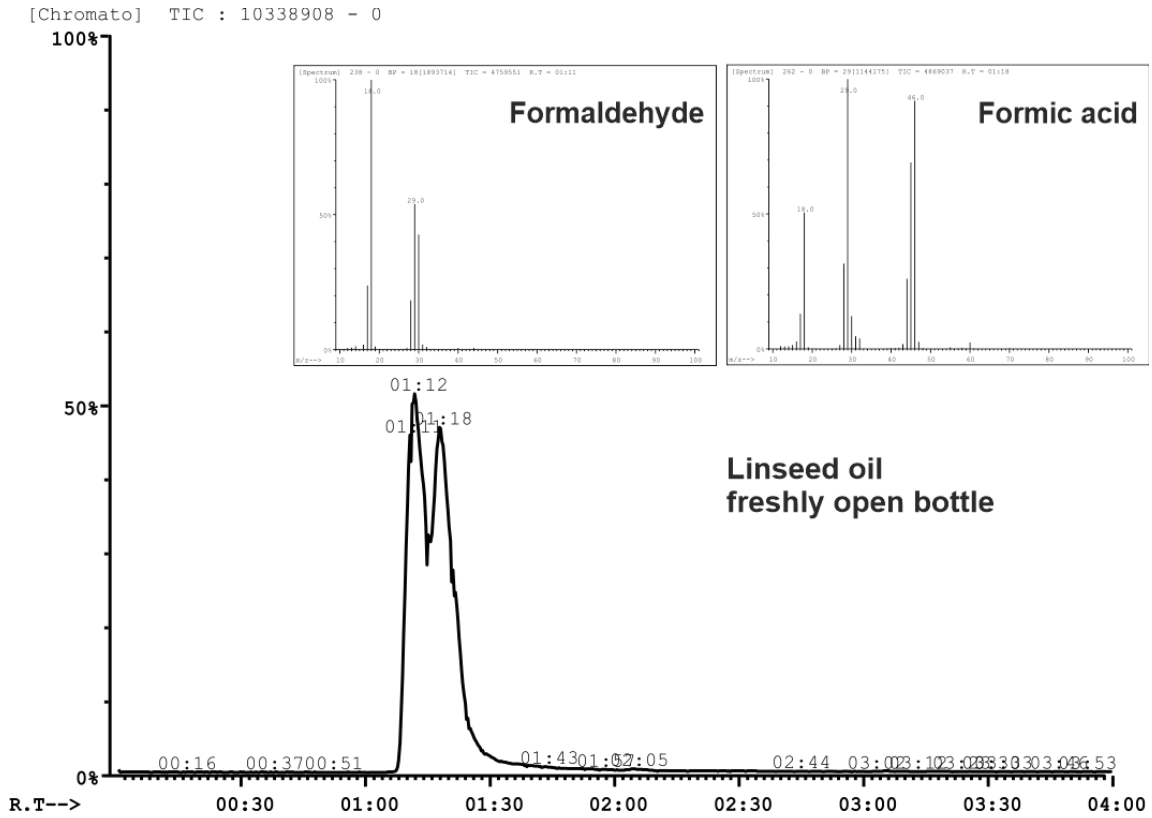

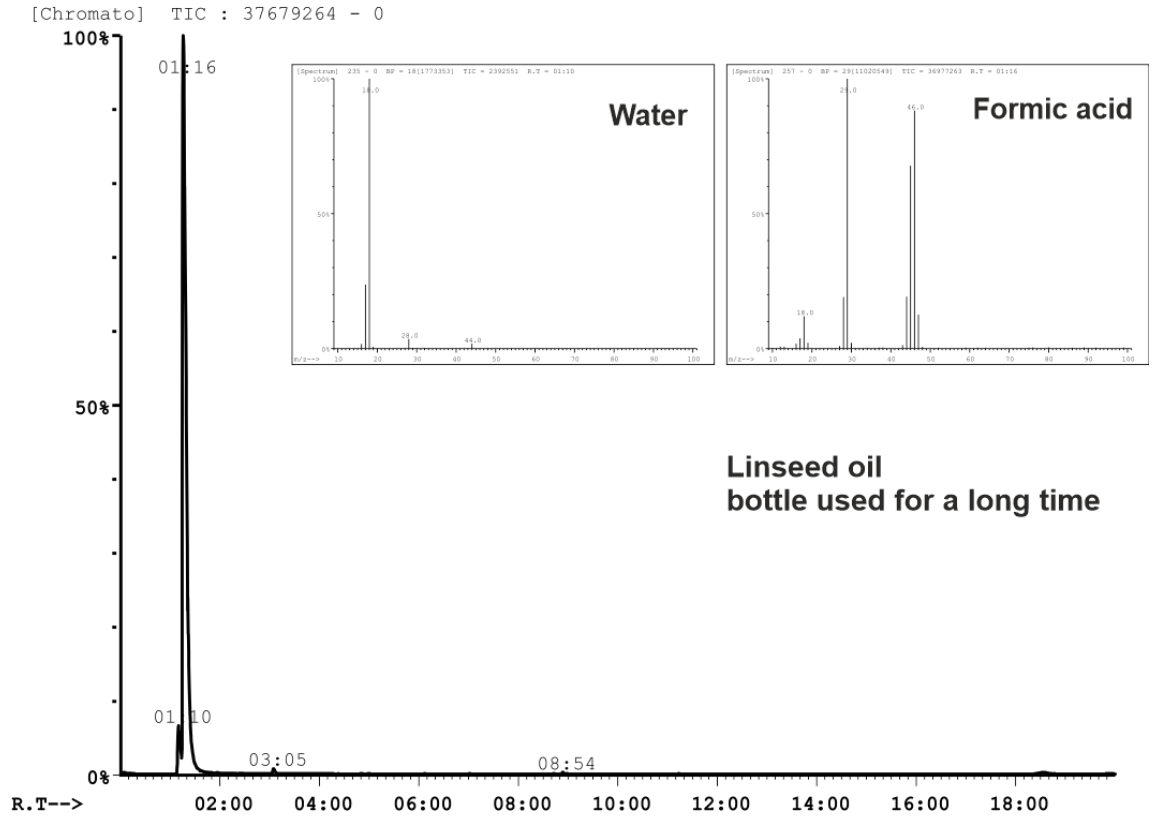

Fig. S6 GC-MS analyses of vapors above linseed oil. The experimental set-up was tailored for the detection of derivatives of methanol and/or water thus other components were not detected.

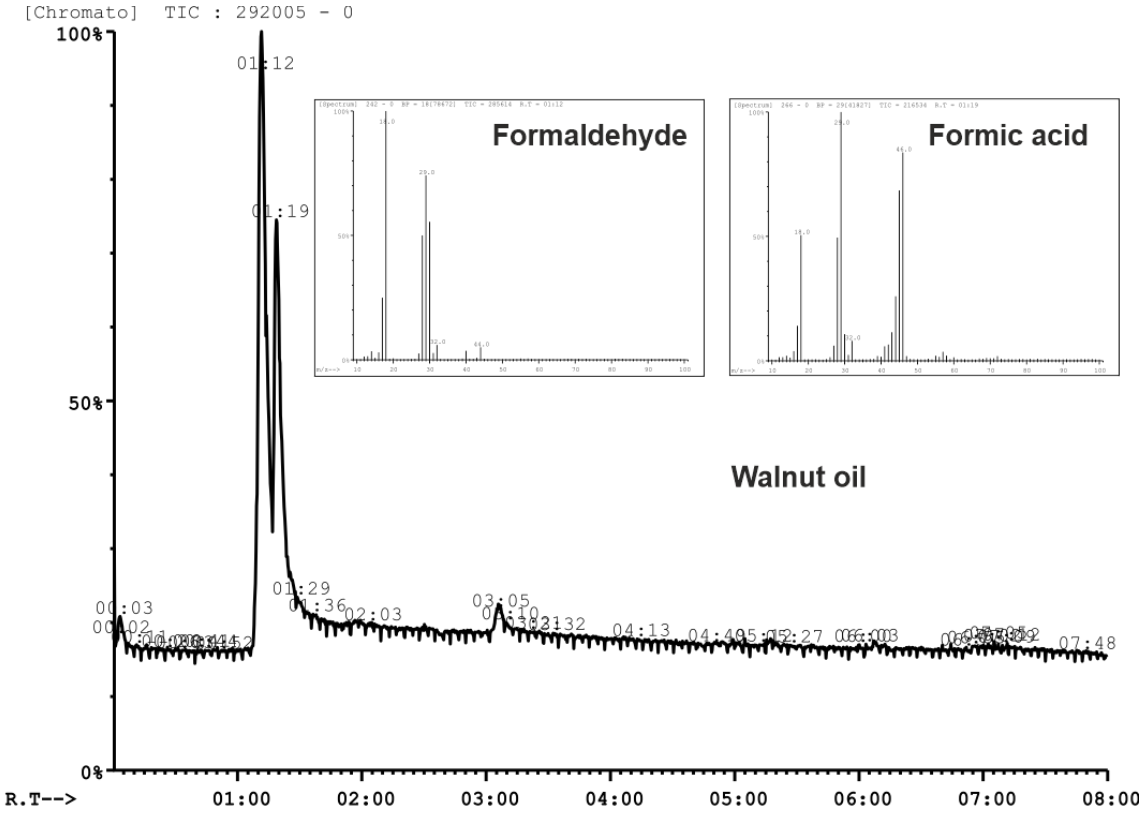

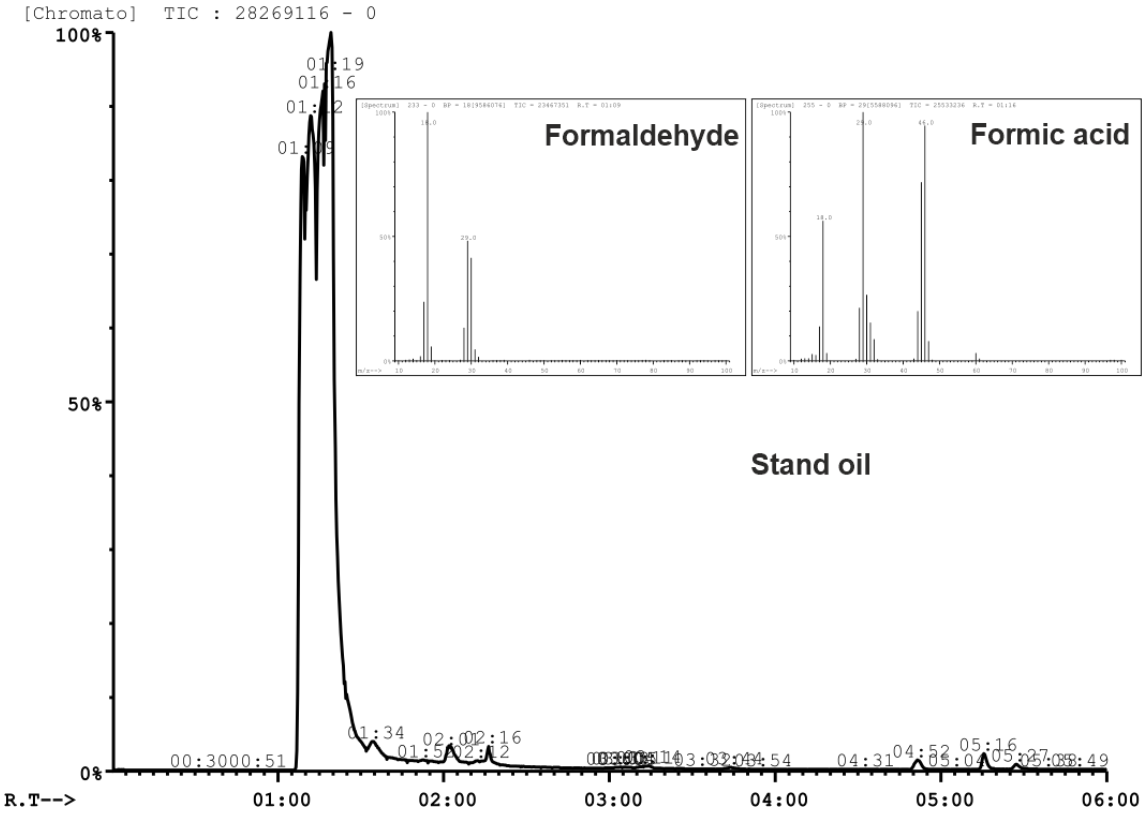

Fig. S7 GC-MS analyses of vapors above walnut oil and standoil. The experimental set-up was tailored for the detection of derivatives of methanol and/or water thus other components were not detected.

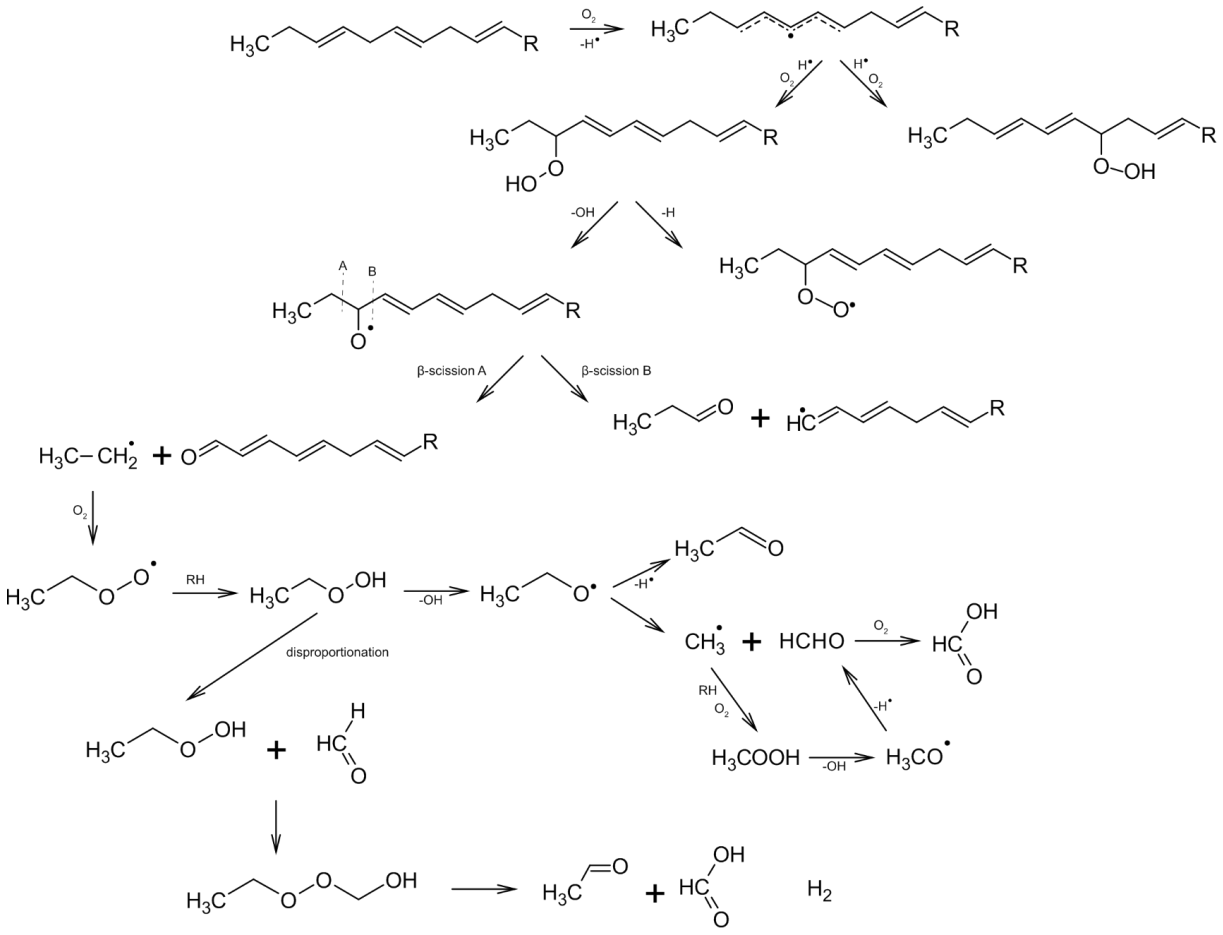

Fig. S8 The reaction scheme of a possible pathway of the formation of formaldehyde and formic acid induced by the autoxidation of oils. For the clarity only the side-chain of the α-linolenic acid is displayed and the reaction of a product of the A-type β-scisson is shown as an example. The scheme is based on the reactions reported in the literature. [10-11]

References

[1] Gavarri J.R., Weigel D, J Solid State Chem, 1975, 13, 252-257
[2] Leinenweber A, Dinnebier R., J. Appl. Cryst, 2010, 43, 17 - 26
[3] ADF2014, *SCM, Theoretical Chemistry*, Vrije Universiteit, Amsterdam, The Netherlands, 2014.
[4] C. Fonseca Guerra, J. G. Snijders, G. te Velde, E. J. Baerends, *Theor. Chem. Acc.* 1998, *99*, 391–403.
[5] G. te Velde, F. M. Bickelhaupt, E. J. Baerends, C. Fonseca Guerra, S. J. A. van Gisbergen, J. G. Snijders, T. Ziegler, *J. Compputational Chem.* 2001, *22*, 931–967.
[6] S. A. Southern, D. Errulat, J. M. Frost, D. L. Bryce, B. Gabidullin, *Faraday Discuss.* 2017, *203*, 165–186.
[7] E. van Lenthe, E. J. Baerends, J. G. Snijders, *J. Chem. Phys.* 1993, *99*, 4597.
[8] E. van Lenthe, E. J. Baerends, J. G. Snijders, *J. Chem. Phys.* 1994, *101*, 9783–9792.
[9] E. van Lenthe, J. G. Snijders, E. J. Baerends, *J. Chemi* 1996, *105*, 650–6516.
[10] H. Wexler, *Chem. Rev.*, 1964, 64, 591–611.
[11] E. N. Frankel, *Prog. Lipid res.*, 1982, 22, 1–33.